Title

Nanoscale Friction of Hydrophilic and Hydrophobic Self-Assembled Monolayers in Water

Journal

Tribology Letters, 68(2)

ISSN

1023-8883

Authors

Yang, Quanpeng
Nanney, Warren
Hu, Xiaoli
et al.

Publication Date

2020-06-01

DOI

10.1007/s11249-020-01301-0

Peer reviewed

Tribology Letters 68 (2020) 63

http://dx.doi.org/10.1007/s11249-020-01301-0

Nanoscale Friction of Hydrophilic and Hydrophobic Self-Assembled Monolayers in Water

Quanpeng Yang,[†] Warren Nanney,[‡] Xiaoli Hu,[†] Tao Ye,[‡] and Ashlie Martini[*,†]

[†]*Department of Mechanical Engineering, University of California-Merced, 5200 N. Lake Road, Merced, California 95343, United States*

[‡]*Department of Chemistry and Chemical Biology, University of California-Merced, 5200 N. Lake Road, Merced, California 95343, United States*

E-mail: amartini@ucmerced.edu

Abstract

Self-assembled monolayers (SAMs) can reduce friction in boundary lubricated contacts by providing a low shear strength interface for sliding. However, the nanoscale mechanisms underlying low friction on SAMs are still not fully understood, especially in liquid environments in which hydrophobility or hydrophilicity affects friction. To understand this effect, friction of SAMs in water was measured using atomic force microscope experiments and molecular dynamics simulations, where hydrophilicity or hydrophobicity was determined by the terminal group of the alkanethiols. The friction on hydrophilic SAMs was larger than that on hydrophobic SAMs in both experiments and simulations, but this trend could not be explained by the strength of the adhesive force between the tip and the SAMs. Instead, analysis of the contributions of the water and SAMs to the total friction force revealed that the difference between the hydrophobic and hydrophilic SAMs could be explained by interactions between the tip and water during sliding. The much larger tip-water force on hydrophilic SAMs was attributed to a dense layer of water that was displaced during sliding as well as hydrogen bonds that formed between the water molecules and hydrophilic SAMs and then broken by the tip as it slid, leading to higher friction force.

INTRODUCTION

Self-assembled monolayers (SAMs) consisting of well-organized, densely packed spacer chains have the potential to solve many practical adhesion- and friction-related problems.[1–3] SAMs are also promising boundary lubricants due to their nanometer thickness, strong bonding to a substrate, variety of possible functional groups that can be incorporated to modify surface energy and frictional properties.[1]

Although many studies have characterized friction on SAMs using macro- and micro-scale experiments (see, for example, [4–10]), research focused on understanding the fundamental mechanisms of friction has been primarily performed using atomic force microscopy (AFM).

AFM-based studies of friction on SAMs have revealed several important frictional properties. For example, odd-even effects have been observed, where SAMs with an odd number of carbon atoms in the alkanethiol chain have larger friction coefficient than SAMs with even numbers of carbon atoms.[11–15] Also, it has been reported that SAMs with shorter chain lengths dissipate more energy during sliding and exhibit higher friction forces.[1,16,17] Studies have shown that the friction between some SAMs is dependent on the pH of the liquid in which they are probed, while others are independent of pH value.[10] Further, friction on SAMs has been reported to depend on sliding direction relative to the SAM orientation, i.e. frictional anisotropy and asymmetry.[18–20] Lastly, it is commonly agreed that friction depends on the hydrophobicity of the SAM terminal group and AFM tip apex.[10,21–31] This observation is the focus in the present research.

Previous AFM-based studies have characterized friction on hydrophobic and hydrophilic SAMs with a variety of different AFM tip materials (Au, Si_3N_4, -OH SAM terminated, -CH_3 SAM terminated), self-assembled monolayers (-OH and -CH_3 terminated), substrates (Au, Si) and solvents (ethanol, hexadecane, methanol, n-decane, water, humid air, dry air).[10,21–37] In some of these studies, friction was measured on hydrophilic and hydrophobic SAMs along the same scan lines on the same substrate.[24,28,29,31–37] With this approach, if SAMs were the same height, the effect of hydrophobicity could be isolated.[24,28,29,33–36] These studies consistently reported that friction decreased as hydrophilic/hydrophilic >hydrophobic/hydrophobic >hydrophilic/hydrophobic, for a given tip/SAM contact. The effect of hydrophobicity on SAMs has also been reported to be velocity dependent where, as sliding velocity increases, friction increases and then reaches a plateau for hydrophobic SAMs and decreases for hydrophilic SAMs.[18] Some previous AFM studies have shown that friction trends are the same as trends observed for adhesion, and it has been proposed that there is a direct correlation between the friction force and adhesion force on SAMs,.[7,10,38] However, adhesion trends on hydrophilic and hydrophobic SAMs in liquid are not consistent in the literature,[4,23,30,39,40] so adhesion may not entirely explain observed friction results.

Despite the large number of experimental studies of the effect of hydrophobicity on SAM friction, there are only a few papers reporting simulations of this phenomenon.[18,23,41–43] These simulations were performed using molecular dynamics (MD) simulation in order to capture the atomic interactions between the AFM tip and SAM chains that underlie measured friction. Previous MD simulations described sliding between two layers of SAMs in water[42,43] or in vacuum,[23] or between a model tip apex and SAM layer in vacuum.[18,41] Importantly, none of the previous simulation studies described tip-SAM friction in a liquid environment, which is important since some experimental studies of SAMs were performed in these conditions.[22,24,28] Further, in the simulations mentioned above, hydrophilic and hydrophobic SAMs were modeled separately in different simulation boxes, which is inconsistent with previous AFM studies where friction was measured on different SAMs in the same scan line.[24,28,29,31–37] Therefore, observations from experiments could not be directly explained by simulation results. Simulations of friction on hydrophilic and hydrophobic SAMs in liquid in the same simulation are needed to complement AFM experiments for the same material system and explain observed trends.

In this work, we performed MD simulations and AFM experiments of atomic scale friction between a nanoscale probe and alkanethiol monolayers terminated with CH_3 (hydrophobic) or OH (hydrophilic) in the presence of water. In both experiments and simulations, hydrophilic and hydrophobic SAMs with the same chain length were positioned next to one another on a gold substrate so that friction could be measured along the same scan line. Both experiments and simulations reproduced the expected result that friction was higher on hydrophilic than hydrophobic SAMs. Then, atomic-scale information available in the simulations was used to understand the observed trends. First, the adhesive forces for both SAMs were calculated. Then, based on the adhesion and friction trends obtained, the individual contributions of the water and the SAMs to the overall force on the tip were characterized. Lastly, the origin of the significant contribution of the tip-water force to the observed friction on hydrophilic SAMs was investigated in terms of the local water distribution and hydrogen

bonding. The results demonstrated the origins of friction on hydrophilic and hydrophobic SAMs, with more general implications for friction measurements in water on other surfaces.

METHODS

Experiments

Monolayer Self Assembly: Unless otherwise stated, all materials were purchased from Fisher Scientific Co. (Pittsburg, PA, USA). Ultrapure water was supplied from a NANOpure Diamond (Barnstead, Lake Balboa, CA, USA) with a resistivity of 18.2 MΩ·cm. All glassware was cleaned with piranha acid (3:1 sulfuric acid: 30% hydrogen peroxide. CAUTION piranha is highly corrosive and reacts violently with organics) rinsed with water and dried with compressed air that was filtered using a Vacu Guard L#S975 filter GE Whatman, Pittsburgh, PA, USA). Au (111) bead substrate was prepared using a previously reported protocol.[44] To form the host self-assembled monolayer, the substrate was cleaned with 70% v/v hot nitric acid (CAUTION: hot nitric acid is highly corrosive and reacts violently with organics), rinsed with water, and flame annealed in a H_2 flame before immersion in 4 mM 11-mercapto-1-undecanol ($C_{11}OH$) (Sigma-Aldrich Co., St. Louis, MO, USA) in the dark and under nitrogen (Praxair Inc., Danbury, CT, USA) for 24 h. Prior to nanografting and imaging, the surface was rinsed with ethanol, then water, and dried with compressed air. The sample was then secured to a custom-made AFM Teflon liquid cell that was cleaned with piranha, rinsed with water, and dried with compressed air. The liquid cell was then attached to a fluid exchange apparatus with 20 GA Teflon tubing (Small Parts Inc, Logansport, IN, USA) consisting of a 7807-10 Digital Pump using Tygon 07MHLLM07 tubing (Ismatec, Wertheim, Germany) that was cleaned by cycling 1M Nitric Acid, water, then DMSO each for 10 minutes at 60 μL/sec.

Nanografting: All nanografting, imaging, and force spectroscopy experiments were performed using an Agilent/Keysight 5500 AFM with a N9524A/B closed loop scanner

(Keysight Technologies, Santa Rosa, CA, U.S.A.) with a modified cantilever deflection sensor system[45] controlled with PicoView 2.10.3 (Keysight Technologies, Santa Rosa, CA, USA). Imaging data was processed with WSxM 5.0.[46] Nanografting was performed in 4 μM 1-dodecanethiol (Sigma-Aldrich Co., St. Louis, MO, USA) in dimethyl sulfoxide (DMSO). The $C_{11}OH$ SAM surface was first imaged with AC-AFM mode using diamond-like-carbon tips (HQ: NSC14/HARD/AL BS μMasch, Sofia, Bulgaria) with a nominal spring constant of 5 N/m and a nominal radius of curvature of 20 nm driven between 40-60 kHz. https://www.overleaf.com/project/5d1d42c10c6d5b2b98a85cd9Grafting was then performed in contact mode with the same tip using deflection as the feedback signal. A custom Python 2.7 control script was used to compensate for laser positional drift between squares, creating a 5x5 array of 200-250 nm^2 squares with 1 μm^2 marker squares used for relocation. Grafting parameters were set to 2 lines/sec with 128 lines/square. Based on the tip radius curvature of 20 nm and SAM thickness of 1.5 nm, thiol molecules within 8 nm of the tip apex could be removed. In our experiment, the line spacing was set to 2 nm and the nanografting was performed in both trace and retrace directions to ensure 100% conversation in the grafted area. Post-grafting, the tip was withdrawn 100 μm leaving the AFM tip and substrate submerged. The substrate was then rinsed using the attached fluid exchange system with DMSO, 50:50 DMSO:water, water, then an imaging buffer solution (pH 7, 170 mM KCl, 10mM 4-(2-hydroxyethyl)-1-piperazineethanesulfonic acid (HEPES)) each for 10 minutes at a rate of 60 μL/sec. The buffer solution ensured constant neutral pH and ionic strength and minimize the variability of double layer force between the tip and the SAM surface.

Friction Imaging: After rinsing, the nanografted SAMs were imaged with a diamond-like-carbon coated tip (HQ: CSC17/HARD/AL BS μMasch, Sofia, Bulgaria) with a nominal spring constant of 0.18 N/m that had been cleaned by soaking in methanol. Seven nanografted squares were imaged across four substrates. Topographical and friction imaging was performed in contact mode at a constant load of $\sim$6.9 nN.

Simulations

The model system, shown in Figure 1, consisted of a half-spherical diamond AFM tip apex and alkanethiol SAMs on gold immersed in water. The gold surface had dimensions of 10.0 nm $\times$ 5.2 nm in the x- and y-directions. The radius of the tip was 1.5 nm. Half of the model SAMs were hydrophilic, terminated with -OH ($-S(CH_2)_{11}OH$) and half were hydrophobic terminated by -CH_3 ($-S(CH_2)_{11}CH_3$). The sulfur head groups of the alkanethiol SAMs formed a $(\sqrt{3} \times \sqrt{3})R30^\circ$ triangular structure on the gold surface. The SAM density of 0.216 nm^2 per chain was consistent with previous experiments and simulations reported in the literature.[47–49]

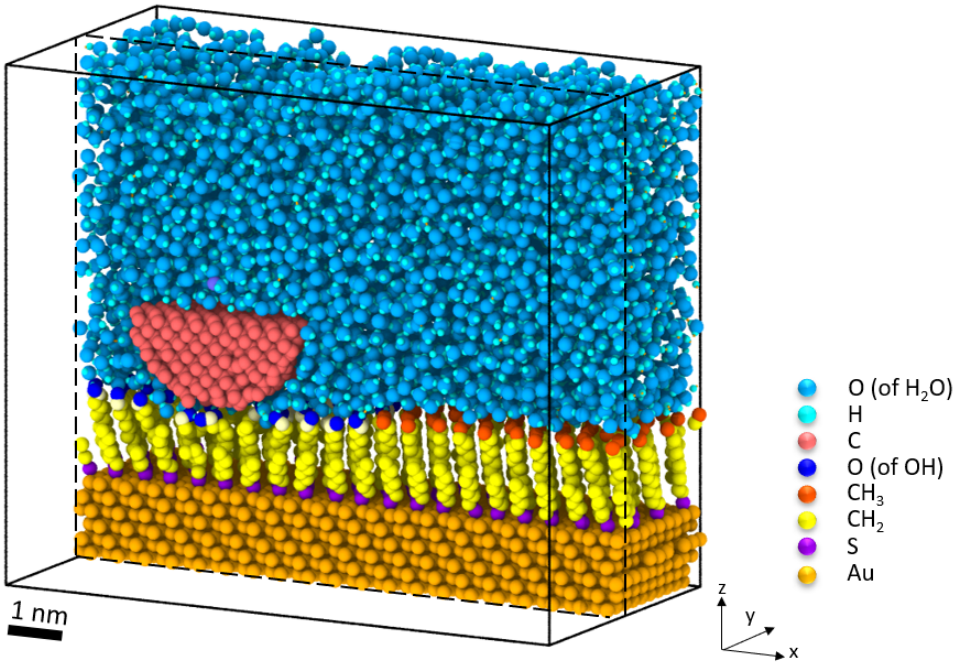

Figure 1: Perspective view of half of the model showing the tip apex in water sliding on hydrophobic and hydrophilic SAMs on a gold surface. The tip slides in the positive x-direction.

The CH_2 and CH_3 groups in the 1-dodecanethiol ($C_{11}CH_3$) and 11-mercapto-1-undecanol ($C_{11}OH$) were treated using a united atom model, in which the mass of hydrogen atoms was added to their corresponding carbon atoms, with parameters from Ref. 50. The partial

charges and potential parameters for the O and H atoms in the hydroxyl terminated $C_{11}OH$ SAMs were obtained from Ref. 51. The interactions within the Au substrate and the tip were defined by the Embedded Atom Method (EAM)[52] and the adaptive intermolecular reactive empirical bond order (AIREBO) potential,[53] respectively. The interactions within water molecules were described by the extended Simple Point Charge potential SPC/E.[54] The Morse potential was used to model the interactions between S and Au atoms.[55,56] Lorentz-Berthelot mixing rules[57] and the Lennard-Jones potential[50] were applied to describe all other long-range interactions. This combination of potentials had been used successfully to model dynamic AFM on SAMs.[58,59]

During simulations, the tip was treated as a rigid body and the bottom 0.1 nm of the gold substrate was fixed. Periodic boundary conditions were applied in the x- and y-directions. Dynamics simulations were performed at a temperature of 300 K in the NVT ensemble (constant number, volume, and temperature) using a Nosé-Hoover thermostat with a 0.01 ps damping factor applied to all unconstrained atoms in the system. All simulations in this work were run using large-scale atomic/molecular massively parallel simulator (LAMMPS) software[60] with a 0.5 fs time step. OVITO[61] was used for visulization.

To simulate sliding friction, the the tip apex was connected to a virtual atom through a harmonic spring with a stiffness of 1.6 N/m in x-direction to simulate the cantilever in an AFM experiment. A normal force between 0.38 and 0.95 nN was applied to the tip. Then the tip apex was dragged by the virtual atom which moved in the x-direction at a speed of 2 m/s. The simulation was repeated 8 times by letting the tip cross the periodic boundaries to begin the next cycle, for a total of 80 nm of sliding. Adhesion was measured in separate simulations where the tip was brought down to the SAMs surface vertically at a normal load of 0.38 nN and left there until its the vertical position was steady. Then, the tip was pulled away from the surface and the maximum negative force during the pull-off process was considered as the adhesion force.

RESULTS AND DISCUSSION

Figure 2 shows representative topography and friction images measured using contact mode AFM. There is no contrast in the topography image, consistent with the fact that the hydrophobic and hydrophilic SAMs are the same height and they are known to have the same density.[62] However, in the friction image there is contrast between the lighter color (higher friction) of the $C_{11}OH$ SAMs and the darker color (lower friction) of the $C_{11}CH_3$ SAMs. The same trend was observed on seven nanografted squares imaged on four different samples. These results are consistent with trends reported in previous experiments that showed hydrophilic SAMs have higher friction than hydrophobic SAMs.[4,32,33]

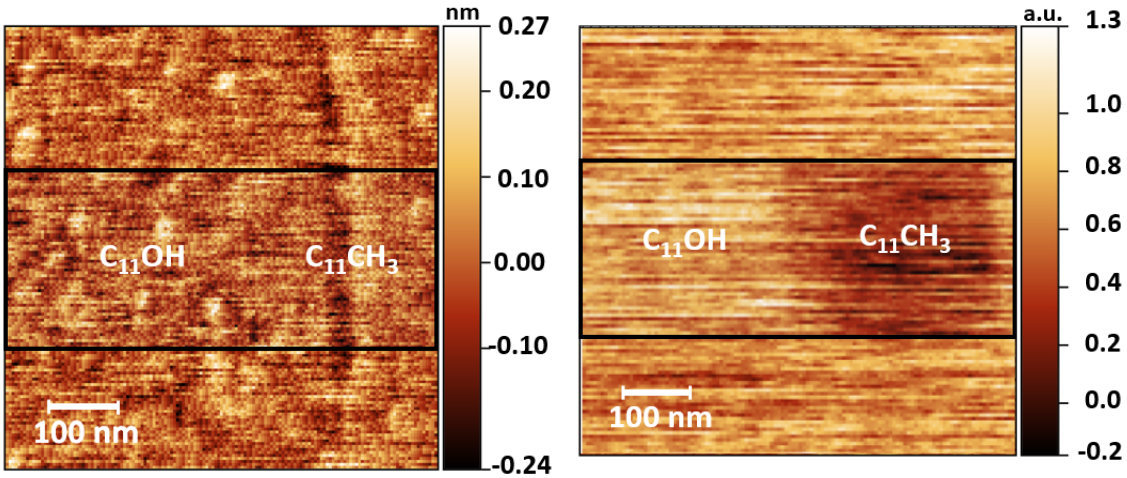

(a) (b)

Figure 2: (a) Topography and (b) friction measured using contact mode AFM of $C_{11}CH_3$ SAMs nanografted into $C_{11}CH_3$ SAMs. The regions identified by black rectangles were used to calculate the average line profiles reported in Figure 3(a).

The friction contrast between the hydrophobic and hydrophilic SAMs can be quantified from average line profiles calculated from the regions identified by the black rectangles in Figure 2 as shown in Figure 3(a). The average friction on the hydrophilic SAMs is ∼60% larger than that on the hydrophobic SAMs. A similar calculation was performed from the simulation data, averaging the topography and friction from eight passes of the tip across the simulation domain. Average simulation topography and friction profiles are shown in

Figure 3(b). Consistent with the experimental results, there is minimal difference in the height of the two SAMs (less than 0.1 nm), but the friction on the $C_{11}OH$ is larger than that on the $C_{11}CH_3$. Note that the transitions between the regions identified as hydrophilic or hydrophobic are large in the simulation because the model tip is only a few times smaller than the lateral dimension of the simulation box, so the tip is effectively sliding on both SAMs during part of each sliding cycle.

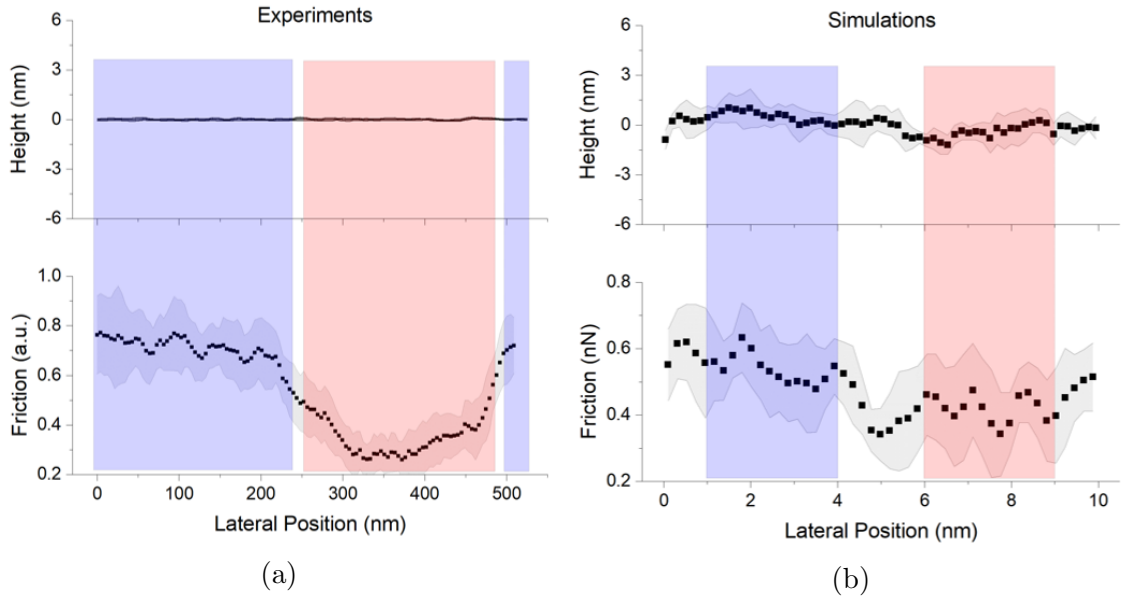

(a) (b)

Figure 3: Average height and friction profiles from (a) experiments and (b) simulations illustrating the contrast between $C_{11}OH$ (blue background) and $C_{11}CH_3$ (red background) SAMs. Symbols represent averages over 15 line traces in experiments and 8 in simulations, and shaded regions reflect the standard deviation of that data at each lateral position. Simulation data corresponds to a normal load of 0.38 nN.

Previous studies have proposed that the difference in friction between hydrophobic and hydrophilic SAMs can be explained by differences in adhesion.[30,63] However, there is inconsistency in the adhesion trends reported previously for $C_{11}OH$ and $C_{11}CH_3$ SAMs in liquid. For example, measurements using a SAM-terminated tip in water reported adhesion decreased as OH/OH > CH3/CH_3 > CH3/OH, which was consistent with the friction trend.[23,30] However, measurements of SAMs probed with a bare AFM tip reported adhesion in water exhibited CH_3 > OH,[4] while in humid air the trend was CH_3 < OH.[39] Lastly, SAMs probed with bare

AFM in ethanol or perfluorodecalin resulted in adhesion trends where OH > CH_3.[40] Therefore, adhesion may explain friction trends in some cases, but not all. Adhesion was measured in our model system using simulations of pull off tests. It was found that the adhesion on $C_{11}OH$ was 0.76 nN while that on $C_{11}CH_3$ was 1.11 nN. This is inconsistent with our friction trend, suggesting the friction contrast was determined by a different mechanism.

To identify other possible explanations of the friction contrast between hydrophilic and hydrophobic SAMs, simulations were performed at a range of normal loads. Figure 4 shows the load dependence of the average friction on the hydrophobic and hydrophilic SAMs. As load increases, friction force on both SAMs increases. Also, at all loads, the total friction force on the $C_{11}OH$ is greater than that on the $C_{11}CH_3$ (between 7 and 20% larger). The origin of this difference can be understood by analyzing the contributions of the tip-water and tip-SAM interactions to the total friction force. First, it can be observed that the tip-SAM force increases with load while the tip-water force remains relatively constant for both SAMs. Considering only the tip-SAM force, Figure 4 shows that the tip-SAM force is larger for the $C_{11}CH_3$ than that for the $C_{11}OH$. To explain this, pull off simulations were repeated without water and it was found that adhesion on $C_{11}CH_3$ was 30% larger that on $C_{11}OH$, consistent with the tip-SAM force trend. However, Figure 4 shows that the tip-water force is hundreds of times larger for the $C_{11}OH$ than the $C_{11}CH_3$; in fact the water contribution is negligible for the $C_{11}CH_3$. Therefore, the greater overall friction for the $C_{11}OH$ is explained by the much larger tip-water force on the hydrophilic SAMs. This tip-water force contribution to friction is analyzed next.

The first possible explanation of the higher tip-water force (and in turn higher friction) on the hydrophilic SAMs is that there are simply more water molecules in the case of the hydrophilic surface that have to be displaced for the tip to slide. This can be quantified from the local density distribution of the water near the two SAM surfaces. The density distribution was calculated from the average number of water molecules in 0.05 nm thick "bins" parallel to the SAM surface for each layer along the vertical direction (z) from the

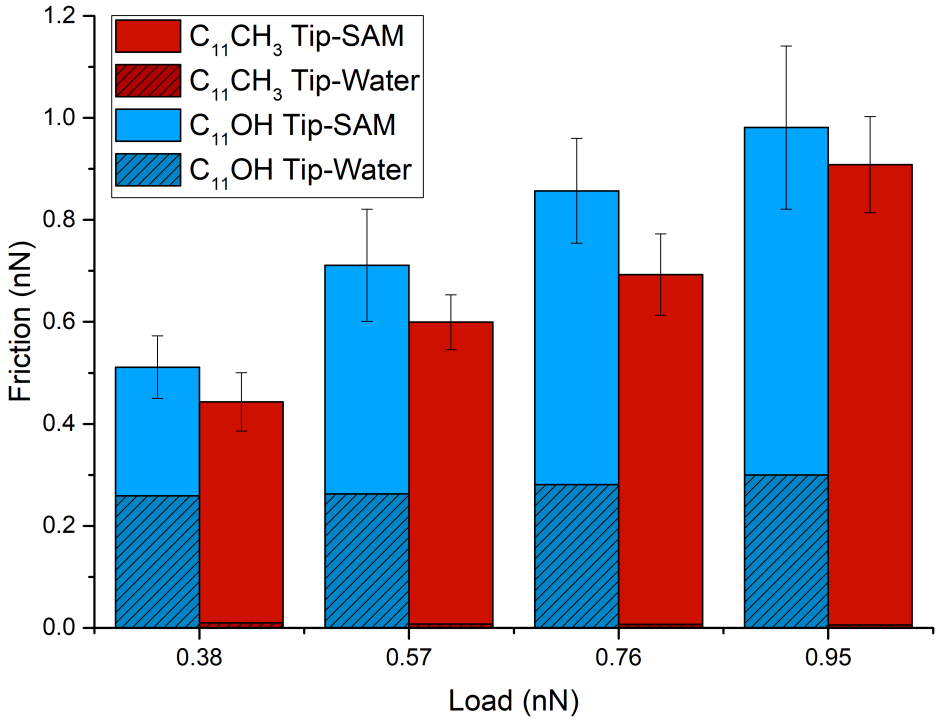

Figure 4: Average friction force from simulations for the $C_{11}OH$ and $C_{11}CH_3$ SAMs as a function of normal load. Averages are calculated over the blue and red shaded regions in Figure 3(b) and error bars correspond to the standard deviation. The contributions of the tip-water and tip-SAM interactions to the total friction force are shown as patterned vs. solid regions, respectively.

SAM surface (z = 0 nm) to the top layer of the simulation box (z = 5.8 nm) as shown in Figure 5. Far from the surface (above ∼0.5 nm), there is no difference in the water density between the two SAMs. However, the density of water near the SAMs surface oscillates with peaks spaced by the diameter of water molecule (∼ 0.275 nm) where the amplitude of oscillations decays exponentially with distance from the surface to approach the bulk water density. These features are attributable to the packing of the liquid molecules being more ordered next to the solid compared to those in the liquid bulk.[64] Lastly, this analysis shows that there is a dense layer of water close to the $C_{11}OH$ surface (z ∼0.25 nm) that is not present in the case of the $C_{11}CH_3$ SAMs. Some of these water molecules are entrained between the tip and SAM and others are in front of the tip where they have to be displaced for sliding to occur. This dense layer therefore likely contributes to the higher tip-water force on the hydrophilic surface (Figure 4) and, in turn, the higher friction. However, considering the region occupied by the tip ($0 < z < 1.5$ nm), there are only 11% more water molecules on $C_{11}OH$ than on $C_{11}CH_3$. This is much less than the huge difference in tip-water force that was observed, which suggests there is another mechanism contributing to the tip-water force on the $C_{11}OH$ SAMs.

Water could contribute to friction on both surfaces because the water molecules have to be displaced by the tip as it slides. However, on the hydrophilic surface, the water molecules can also form hydrogen bonds with the SAM surface which then have to be broken for the tip to slide. Hydrogen bonding exists on the hydrophilic SAMs either as HO_{SAM}-H_{water} or H_{SAM}-OH_{water}, as illustrated in Figure 6(a). H-bonds were identified in the simulation based on the HO-O angle, O-O distance and O-H distance, using the criterion reported previously.[65,66] The formation and breaking of H-bonds occur dynamically throughout the simulation, so individual bond breaking events cannot be correlated to the friction signal. Therefore, to analyze the contribution of hydrogen bonding, the number of bonds was tracked as a function of lateral position of the tip. The formation and breaking of H-bonds occurs dynamically throughout the simulation, so individual bond breaking events cannot be correlated to the

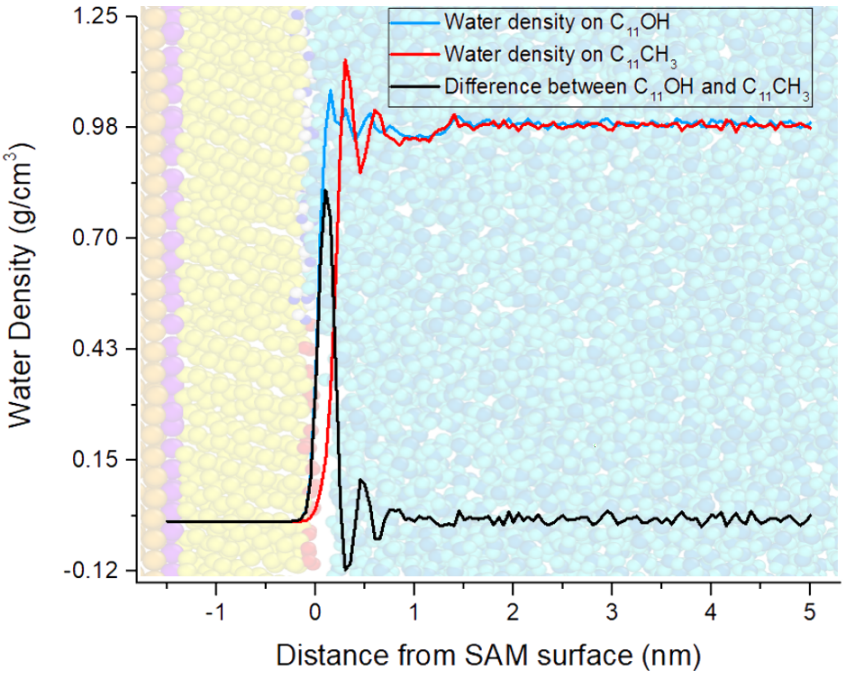

Figure 5: Water density distribution on $C_{11}OH$ and $C_{11}CH_3$ SAMs, and the difference in density between the $C_{11}OH$ and $C_{11}CH_3$. A faded side-view snapshot of the model system is shown in the background to facilitate correlation between the calculated density and atom positions. The water depletion layer is thicker on the CH_3 terminated SAMs than the OH terminated SAMs.

friction signal. Therefore, to analyze the contribution of hydrogen bonding, the number of bonds was tracked as a function of lateral position of the tip. When the tip was on the CH_3-terminated SAMs, there were an average of 178 H-bonds between the water and OH-terminated SAMs; however, when the tip was sliding on the OH-terminated SAMs, that average decreased to 163. The difference reflects the number of H-bonds broken as the tip slides on the hydrophilic surface. The force required to break these H-bonds therefore likely contributed to the resistance to sliding experienced by the tip.

To test the theory that H-bonds contribute to the larger tip-water force on the hydrophilic SAM, which in turn causes higher friction, simulations were run at different temperatures. According to the literature,[67–69] higher temperature can lead to fewer H-bonds. This relationship between H-bonds and temperature can also be derived from the Langmuir adsorption model.[70,71] When adsorption and desorption processes come to an equilibrium, the rate of adsorption and the rate of desorption are equal and the adsorbate coverage on a surface decreases with increasing temperature. As shown in Figure 6(b), the number of H-bonds decreases with increasing temperature, and more H-bonds mean more water molecules are adsorbed on the $C_{11}OH$ surface, consistent with the theoretical prediction. The tip-water force was also calculated as a function of temperature and it was observed to decrease with temperature for the $C_{11}OH$ SAMs and increase slightly on the $C_{11}CH_3$ SAMs (Figure 6(b)). The decrease in the hydrophilic case is explained by there being fewer water molecules adsorbed to the surface for which H-bonds have to be broken for sliding to occur. The slight increase for the hydrophobic SAMs may be due to an increase in the number of water molecules that have to be displaced further from the surface caused by desorption that increases with temperature. This analysis demonstrates that friction on the hydrophilic SAMs is increased by the presence of H-bonds that form between water molecules and the terminal groups that act to resist sliding.

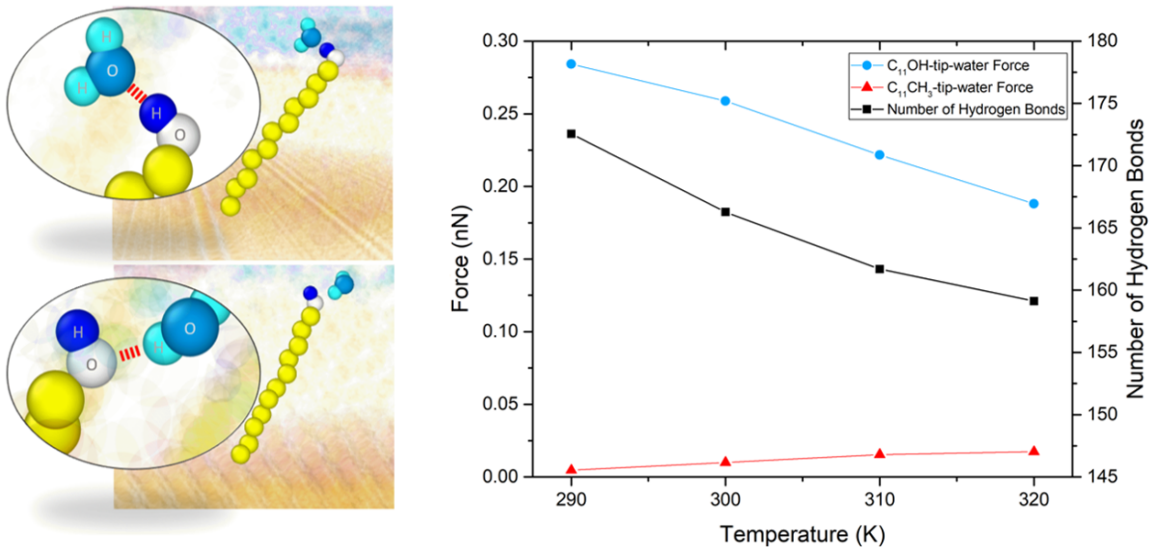

(a) (b)

Figure 6: (a) Snapshots from the simulation of two H-bonds that are present on the hydrophilic surface, where all atoms except those of interest are faded out for clarity. (b) Tip-water force and number of H-bonds on the $C_{11}OH$ SAMs decrease as temperature increases, while there is a slight increase in the tip-water force on the $C_{11}CH_3$ SAMs.

Conclusion

In this study, experiments and MD simulations were performed to study the friction of hydrophilic ($C_{11}OH$) and hydrophobic ($C_{11}CH_3$) SAMs of equal heights measured along the same scan line. Higher friction was observed for $C_{11}OH$ compared to ceC11CH3 in both experiments and simulations. Simulations of pull-off tests showed that, contrary to previous suggestions, adhesion could not explain the observed friction difference. By breaking down the total friction force acting on the tip into tip-SAM force and tip-water force, it was found that the tip-SAM force of $C_{11}OH$ SAMs was greater than the tip-SAM force of $C_{11}CH_3$. However, the more significant difference was observed for the tip-water force, which was measured to be much larger for $C_{11}OH$ than $C_{11}CH_3$. This difference in tip-water force therefore explained the higher friction for the $C_{11}OH$ SAMs.

To explore why the tip-water force was larger for $C_{11}OH$, the local water density was analyzed. It was found that the water density was only different near the water-SAM inter-

face, where there was more water closer to the $C_{11}OH$. However, the difference in number of water molecules was relatively small compared to the difference in tip-water friction force, suggesting the friction contrast was not solely due to entrainment or displacement of more water molecules on the hydrophilic SAMs. Instead, it was proposed that the water forms H-bonds with the hydrophilic surface that have to be broken for sliding to occur. To test this hypothesis, simulations were repeated at different temperatures. As temperature increased, the number of H-bonds decreased on $C_{11}OH$, consistent with theoretical predictions, and the $C_{11}OH$-tip-water force decreased correspondingly. This indicated that H-bonds between the water molecules and hydrophilic SAMs indeed contributed to the tip-water force and, in turn, the higher friction. This understanding of the effect of hydrophobicity on friction of SAMs in water is important to MEMS/NEMS, particularly, bio-MEMS/NEMS that are likely to operate in liquid environments. Moreover, achieving reproducible atomic resolution in aqueous environment with AFM is still a challenge[72] and insights from the present study may help understand the origin of the atomic scale contrast and inform new ways to improve the reproducibility of atomic resolution imaging.

Acknowledgements

This research was supported by the National Science Foundation through Grant # CHE 1808213 and the NASA Merced nAnomaterials Center for Energy and Sensing (MACES) through the support of the National Aeronautics and Space Administration (NASA) grant no. NNX15AQ01.

References

(1) Cheng, H.; Hu, Y. Influence of chain ordering on frictional properties of self-assembled monolayers (SAMs) in nano-lubrication. *Advances in colloid and interface science* **2012**, *171*, 53–65.

(2) Bhushan, B. *Nanotribology and Nanomechanics I: Measurement Techniques and Nanomechanics*; Springer Science & Business Media, 2011; Vol. 1.

(3) Chaudhury, M. K. Adhesion and friction of self-assembled organic monolayers. *Current opinion in colloid & interface science* **1997**, *2*, 65–69.

(4) Lee, S.; Heeb, R.; Venkataraman, N. V.; Spencer, N. D. Macroscopic tribological testing of alkanethiol self-assembled monolayers (SAMs): pin-on-disk tribometry with elastomeric sliding contacts. *Tribology Letters* **2007**, *28*, 229–239.

(5) Bhushan, B. Self-assembled monolayers (SAMs) for controlling adhesion, friction, and wear. *Springer Handbook of Nanotechnology* **2007**, 1379–1416.

(6) Lio, A.; Charych, D.; Salmeron, M. Comparative atomic force microscopy study of the chain length dependence of frictional properties of alkanethiols on gold and alkylsilanes on mica. *The Journal of Physical Chemistry B* **1997**, *101*, 3800–3805.

(7) Zhang, L.; Li, L.; Chen, S.; Jiang, S. Measurements of friction and adhesion for alkyl monolayers on Si (111) by scanning force microscopy. *Langmuir* **2002**, *18*, 5448–5456.

(8) Barattin, R.; Voyer, N. Chemical modifications of AFM tips for the study of molecular recognition events. *Chemical communications* **2008**, 1513–1532.

(9) Hu, X.; Martini, A. Atomistic simulation of the effect of roughness on nanoscale wear. *Computational Materials Science* **2015**, *102*, 208–212.

(10) Noy, A.; Vezenov, D. V.; Lieber, C. M. Chemical force microscopy. *Annual Review of Materials Science* **1997**, *27*, 381–421.

(11) Mikulski, P. T.; Herman, L. A.; Harrison, J. A. Odd and even model self-assembled monolayers: links between friction and structure. *Langmuir* **2005**, *21*, 12197–12206.

(12) Shaporenko, A.; Brunnbauer, M.; Terfort, A.; Grunze, M.; Zharnikov, M. Structural forces in self-assembled monolayers: Terphenyl-substituted alkanethiols on noble metal substrates. *The Journal of Physical Chemistry B* **2004**, *108*, 14462–14469.

(13) Ramin, L.; Jabbarzadeh, A. Frictional properties of two alkanethiol self assembled monolayers in sliding contact: Odd-even effects. *The Journal of chemical physics* **2012**, *137*, 174706.

(14) Tao, F.; Bernasek, S. L. Understanding odd- even effects in organic self-assembled monolayers. *Chemical reviews* **2007**, *107*, 1408–1453.

(15) Ramin, L.; Jabbarzadeh, A. Effect of water on structural and frictional properties of self assembled monolayers. *Langmuir* **2013**, *29*, 13367–13378.

(16) Prathima, N.; Harini, M.; Rai, N.; Chandrashekara, R.; Ayappa, K.; Sampath, S.; Biswas, S. Thermal study of accumulation of conformational disorders in the self-assembled monolayers of C8 and C18 alkanethiols on the Au (111) surface. *Langmuir* **2005**, *21*, 2364–2374.

(17) Leng, Y.; Jiang, S. Atomic indentation and friction of self-assembled monolayers by hybrid molecular simulations. *The Journal of Chemical Physics* **2000**, *113*, 8800–8806.

(18) Zhang, L.; Leng, Y.; Jiang, S. Tip-based hybrid simulation study of frictional properties of self-assembled monolayers: effects of chain length, terminal group, scan direction, and scan velocity. *Langmuir* **2003**, *19*, 9742–9747.

(19) Liley, M.; Gourdon, D.; Stamou, D.; Meseth, U.; Fischer, T. M.; Lautz, C.; Stahlberg, H.; Vogel, H.; Burnham, N. A.; Duschl, C. Friction Anisotropy and Asymmetry of a Compliant Monolayer Induced by a Small Molecular Tilt. *Science* **1998**, *280*, 273–275.

(20) Jabbarzadeh, A. Friction anisotropy and asymmetry in self assembled monolayers. *Tribology International* **2016**, *102*, 600–607.

(21) Brewer, N. J.; Foster, T. T.; Leggett, G. J.; Alexander, M. R.; McAlpine, E. Comparative investigations of the packing and ambient stability of self-assembled monolayers of alkanethiols on gold and silver by friction force microscopy. *The Journal of Physical Chemistry B* **2004**, *108*, 4723–4728.

(22) Li, L.; Chen, S.; Jiang, S. Nanoscale frictional properties of mixed alkanethiol self-assembled monolayers on Au (111) by scanning force microscopy: humidity effect. *Langmuir* **2003**, *19*, 666–671.

(23) Leng, Y.; Jiang, S. Dynamic simulations of adhesion and friction in chemical force microscopy. *Journal of the American Chemical Society* **2002**, *124*, 11764–11770.

(24) Noy, A.; Sanders, C. H.; Vezenov, D. V.; Wong, S. S.; Lieber, C. M. Chemically-sensitive imaging in tapping mode by chemical force microscopy: relationship between phase lag and adhesion. *Langmuir* **1998**, *14*, 1508–1511.

(25) Clear, S. C.; Nealey, P. F. Chemical force microscopy study of adhesion and friction between surfaces functionalized with self-assembled monolayers and immersed in solvents. *Journal of colloid and interface science* **1999**, *213*, 238–250.

(26) Fujihira, M.; Tani, Y.; Furugori, M.; Akiba, U.; Okabe, Y. Chemical force microscopy of self-assembled monolayers on sputtered gold films patterned by phase separation. *Ultramicroscopy* **2001**, *86*, 63–73.

(27) López-Santos, C.; Yubero, F.; Cotrino, J.; González-Elipe, A. Lateral and in-depth distribution of functional groups on diamond-like carbon after oxygen plasma treatments. *Diamond and Related Materials* **2011**, *20*, 49–56.

(28) Noy, A.; Frisbie, C. D.; Rozsnyai, L. F.; Wrighton, M. S.; Lieber, C. M. Chemical force microscopy: exploiting chemically-modified tips to quantify adhesion, friction, and functional group distributions in molecular assemblies. *Journal of the American Chemical Society* **1995**, *117*, 7943–7951.

(29) Wong, S. S.; Woolley, A. T.; Joselevich, E.; Cheung, C. L.; Lieber, C. M. Covalently-functionalized single-walled carbon nanotube probe tips for chemical force microscopy. *Journal of the American Chemical Society* **1998**, *120*, 8557–8558.

(30) Takano, H.; Kenseth, J. R.; Wong, S.-S.; O'Brie, J. C.; Porter, M. D. Chemical and biochemical analysis using scanning force microscopy. *Chemical Reviews* **1999**, *99*, 2845–2890.

(31) van der Vegte, E. W.; Hadziioannou, G. Scanning force microscopy with chemical specificity: an extensive study of chemically specific tip- surface interactions and the chemical imaging of surface functional groups. *Langmuir* **1997**, *13*, 4357–4368.

(32) Te Riet, J.; Smit, T.; Gerritsen, J. W.; Cambi, A.; Elemans, J. A.; Figdor, C. G.; Speller, S. Molecular friction as a tool to identify functionalized alkanethiols. *Langmuir* **2010**, *26*, 6357–6366.

(33) Wilbur, J. L.; Biebuyck, H. A.; MacDonald, J. C.; Whitesides, G. M. Scanning force microscopies can image patterned self-assembled monolayers. *Langmuir* **1995**, *11*, 825–831.

(34) Tocha, E.; Schönherr, H.; Vancso, G. J. Quantitative nanotribology by AFM: a novel universal calibration platform. *Langmuir* **2006**, *22*, 2340–2350.

(35) Alsteens, D.; Dague, E.; Rouxhet, P. G.; Baulard, A. R.; Dufrêne, Y. F. Direct measurement of hydrophobic forces on cell surfaces using AFM. *Langmuir* **2007**, *23*, 11977–11979.

(36) Vezenov, D. V.; Noy, A.; Rozsnyai, L. F.; Lieber, C. M. Force titrations and ionization state sensitive imaging of functional groups in aqueous solutions by chemical force microscopy. *Journal of the American Chemical Society* **1997**, *119*, 2006–2015.

(37) Chong, K. S.; Sun, S.; Leggett, G. J. Measurement of the kinetics of photo-oxidation of self-assembled monolayers using friction force microscopy. *Langmuir* **2005**, *21*, 3903–3909.

(38) Beake, B.; Leggett, G. Friction and adhesion of mixed self-assembled monolayers studied by chemical force microscopy. *Physical Chemistry Chemical Physics* **1999**, *1*, 3345–3350.

(39) Liu, L. Measurements of Friction and Adhesion for Alkyl Monolayers on Si (111) by Scanning Force Microscopy. **2002**,

(40) Colburn, T. J.; Leggett, G. J. Influence of solvent environment and tip chemistry on the contact mechanics of tip- sample interactions in friction force microscopy of self-assembled monolayers of mercaptoundecanoic acid and dodecanethiol. *Langmuir* **2007**, *23*, 4959–4964.

(41) Jiang, S. Molecular simulation studies of self-assembled monolayers of alkanethiols on Au (111). *Molecular physics* **2002**, *100*, 2261–2275.

(42) Zhang, L.; Jiang, S. Molecular simulation study of nanoscale friction for alkyl monolayers on Si (111). *The Journal of Chemical Physics* **2002**, *117*, 1804–1811.

(43) Zhang, L.; Jiang, S. Molecular simulation study of nanoscale friction between alkyl monolayers on Si (111) immersed in solvents. *The Journal of chemical physics* **2003**, *119*, 765–770.

(44) Clavilier, J.; Faure, R.; Guinet, G.; Durand, R. Preparation of monocrystalline Pt microelectrodes and electrochemical study of the plane surfaces cut in the direction

of the {111} and {110} planes. *Journal of Electroanalytical Chemistry and Interfacial Electrochemistry* **1980**, *107*, 205–209.

(45) Fukuma, T.; Kimura, M.; Kobayashi, K.; Matsushige, K.; Yamada, H. Development of low noise cantilever deflection sensor for multienvironment frequency-modulation atomic force microscopy. *Review of Scientific Instruments* **2005**, *76*, 053704.

(46) Horcas, I.; Fernández, R.; Gomez-Rodriguez, J.; Colchero, J.; Gómez-Herrero, J.; Baro, A. WSXM: a software for scanning probe microscopy and a tool for nanotechnology. *Review of scientific instruments* **2007**, *78*, 013705.

(47) Ghorai, P. K.; Glotzer, S. C. Molecular dynamics simulation study of self-assembled monolayers of alkanethiol surfactants on spherical gold nanoparticles. *The Journal of Physical Chemistry C* **2007**, *111*, 15857–15862.

(48) Hinterwirth, H.; Kappel, S.; Waitz, T.; Prohaska, T.; Lindner, W.; Lammerhofer, M. Quantifying thiol ligand density of self-assembled monolayers on gold nanoparticles by inductively coupled plasma–mass spectrometry. *ACS nano* **2013**, *7*, 1129–1136.

(49) Majumdar, S.; Sierra-Suarez, J. A.; Schiffres, S. N.; Ong, W.-L.; Higgs III, C. F.; McGaughey, A. J.; Malen, J. A. Vibrational mismatch of metal leads controls thermal conductance of self-assembled monolayer junctions. *Nano letters* **2015**, *15*, 2985–2991.

(50) Ong, W.-L.; Majumdar, S.; Malen, J. A.; McGaughey, A. J. Coupling of organic and inorganic vibrational states and their thermal transport in nanocrystal arrays. *The Journal of Physical Chemistry C* **2014**, *118*, 7288–7295.

(51) Hautman, J.; Bareman, J. P.; Mar, W.; Klein, M. L. Molecular dynamics investigations of self-assembled monolayers. *Journal of the Chemical Society, Faraday Transactions* **1991**, *87*, 2031–2037.

(52) Grochola, G.; Russo, S. P.; Snook, I. K. On fitting a gold embedded atom method potential using the force matching method. *The Journal of chemical physics* **2005**, *123*, 204719.

(53) Stuart, S. J.; Tutein, A. B.; Harrison, J. A. A reactive potential for hydrocarbons with intermolecular interactions. *The Journal of chemical physics* **2000**, *112*, 6472–6486.

(54) Berendsen, H.; Grigera, J.; Straatsma, T. The missing term in effective pair potentials. *Journal of Physical Chemistry* **1987**, *91*, 6269–6271.

(55) Mahaffy, R.; Bhatia, R.; Garrison, B. J. Diffusion of a butanethiolate molecule on a Au {111} surface. *The Journal of Physical Chemistry B* **1997**, *101*, 771–773.

(56) Sung, I.-H.; Kim, D.-E. Molecular dynamics simulation study of the nano-wear characteristics of alkanethiol self-assembled monolayers. *Applied Physics A* **2005**, *81*, 109–114.

(57) Allen, M. P.; Tildesley, D. J. *Computer simulation of liquids*; Oxford university press, 2017.

(58) Hu, X.; Nanney, W.; Umeda, K.; Ye, T.; Martini, A. Combined Experimental and Simulation Study of Amplitude Modulation Atomic Force Microscopy Measurements of Self-Assembled Monolayers in Water. *Langmuir* **2018**, *34*, 9627–9633.

(59) Hu, X.; Yang, Q.; Ye, T.; Martini, A. Simulation of Dynamic Atomic Force Microscopy Measurements of Hydrophilic Self-Assembled Monolayers in Water. *Langmuir* **2020**, *36*, 2240–2246.

(60) Plimpton, S. Fast parallel algorithms for short-range molecular dynamics. *Journal of computational physics* **1995**, *117*, 1–19.

(61) Stukowski, A. Visualization and analysis of atomistic simulation data with OVITO–the Open Visualization Tool. *Modelling and Simulation in Materials Science and Engineering* **2009**, *18*, 015012.

(62) Takami, T.; Delamarche, E.; Michel, B.; Gerber, C.; Wolf, H.; Ringsdorf, H. Recognition of Individual Tail Groups in Self-Assembled Monolayers. *Langmuir* **1995**, *11*, 3876–3881.

(63) Schönherr, H.; Hruska, Z.; Vancso, G. J. Surface characterization of oxyfluorinated isotactic polypropylene films: Scanning force microscopy with chemically modified probes and contact angle measurements. *Macromolecules* **1998**, *31*, 3679–3685.

(64) Mate, C. M.; Carpick, R. W. *Tribology on the small scale: a modern textbook on friction, lubrication, and wear Second Edition*; Oxford University Press, 2019.

(65) Luzar, A.; Chandler, D. Structure and hydrogen bond dynamics of water–dimethyl sulfoxide mixtures by computer simulations. *The Journal of chemical physics* **1993**, *98*, 8160–8173.

(66) Guardia, E.; Martí, J.; García-Tarrés, L.; Laria, D. A molecular dynamics simulation study of hydrogen bonding in aqueous ionic solutions. *Journal of Molecular Liquids* **2005**, *117*, 63–67.

(67) Rapaport, D. Hydrogen bonds in water: Network organization and lifetimes. *Molecular Physics* **1983**, *50*, 1151–1162.

(68) Mizan, T. I.; Savage, P. E.; Ziff, R. M. Temperature dependence of hydrogen bonding in supercritical water. *The Journal of Physical Chemistry* **1996**, *100*, 403–408.

(69) Starr, F. W.; Nielsen, J. K.; Stanley, H. E. Fast and slow dynamics of hydrogen bonds in liquid water. *Physical Review Letters* **1999**, *82*, 2294.

(70) Langmuir, I. The constitution and fundamental properties of solids and liquids. Part I. Solids. *Journal of the American chemical society* **1916**, *38*, 2221–2295.

(71) Langmuir, I. The constitution and fundamental properties of solids and liquids. II. Liquids. *Journal of the American chemical society* **1917**, *39*, 1848–1906.

(72) Akrami, S.; Nakayachi, H.; Watanabe-Nakayama, T.; Asakawa, H.; Fukuma, T. Significant improvements in stability and reproducibility of atomic-scale atomic force microscopy in liquid. *Nanotechnology* **2014**, *25*, 455701.